ADVANCED FUNCTIONAL MATERIALS
www.afm-journal.de

Nanomaterial-Based Fluorescent DNA Analysis: A Comparative Study of the Quenching Effects of Graphene Oxide, Carbon Nanotubes, and Gold Nanoparticles

Fan Li, Hao Pei, Lihua Wang, Jianxin Lu, Jimin Gao,* Bowei Jiang, Xingchun Zhao, and Chunhai Fan**

A variety of nanomaterials have shown extraordinarily high quenching ability toward a broad range of fluorophores. Recently, there has been intense interest in developing new tools for fluorescent DNA analysis in solution or inside the cell based on this property, and by exploiting interactions between these nanoscale "superquenchers" and DNA molecules in the single-stranded (ss-) or double-stranded (ds-) forms. Here, a comparative study on the nanoqueching effects is performed by using a series of nanomaterials with different dimensions, i.e., gold nanoparticles (AuNPs, 0D), carbon nanotubes (CNTs, 1D), and graphene oxide (GO, 2D). The quenching efficiency, kinetics, differentiation ability, and influencing factors such as concentration and ionic strength are studied. Interestingly, GO exhibits superior quenching abilities to the other two materials in both the quenching efficiency and kinetics. As a result, a GO-based fluorescent sensor, designed in a simple mix-and-detect format, can detect concentrations of DNA as low as 0.2 nM, which is better than either CNTs or AuNPs by an order of magnitude. This sensor can also differentiate single-base mismatches much better than either CNTs- or AuNPs- based sensors. This study paves the way to better choice of nanomaterials for bioanalysis and elaborate design of biosensors for both in vitro diagnosis and in vivo bioimaging.

1. Introduction

There has been increasing interest in developing molecular and nanoscale probes for studying biomolecular interactions including DNA/RNA hybridization, protein-protein or protein-DNA interactions. Fluorescent molecular probes are a type of versatile approaches for such purposes, including Taqman,[1] molecular beacons,[2,3] and fluorescence signaling aptamers.[4,5] These molecular probes exploit highly specific molecular recognition abilities of biomolecules, e.g., antibody-antigen binding and DNA base paring, which are transduced to measurable fluorescence readout. A typical design of nucleic acid probes involves the labeling of oligonucleotides with a fluorescent dye-quencher pair. Fluorescence resonance energy transfer (FRET) of this pair is coupled with the conformational variation of the oligonucleotides, i.e., binding-induced conformational changes alter the distances between the dye and the quencher, resulting in the change of the fluorescence intensity (FL intensity). The efficiency of these molecular probes is, nevertheless, highly dependent on several factors including the selection and optimization of dye-quencher pairs, and labeling and purification of the pairs on oligonucleotides.

Rapid advances of nanotechnology have exerted great influence on DNA detection technologies since the 1990s.[5–17] There have been a plethora of studies on constructing nano/biointerfaces with electrically, optically and thermally active nanomaterials (NMs) for advancing biomedicine,[18] bioactuated devices,[19,20] biodetection,[21–23] and diagnostics.[24,25] More recently, a range of nanomaterials have been found to be "superquenchers" with ultrahigh quenching efficiency for a wide spectrum of fluorescent dyes due to the prominent nanoscale-surface energy transfer (NSET) effect.[26–29] These nanomaterials include zero-dimensional (0D) gold nanoparticles (AuNPs), 1D single-walled carbon nanotubes (SWNTs), and 2D graphene oxide (GO).[30–33] AuNPs with prominent plasmonic properties have been well known to be biocompatible and can be readily conjugated with various proteins and nucleic acids.[34,35] SWNTs are highly conductive nanomaterials that have been actively exploited for their biosensing and drug delivery properties.[36–38] The recently discovered graphene is a one-atom-thick 2D nanomaterial with extraordinary electronic,

F. Li, H. Pei, Prof. L. Wang, Prof. C. Fan
Laboratory of Physical Biology
Shanghai Institute of Applied Physics
Chinese Academy of Sciences
Shanghai 201800, China
E-mail: fchh@sinap.ac.cn; wanglihua@sinap.ac.cn
Prof. J. Lu, Pof. J. Gao
Key Laboratory of Laboratory Medicine
Ministry of Education
Wenzhou Medical College
Wenzhou 325035, Zhejiang, China
E-mail: jimingao@yahoo.com
B. Jiang, X. Zhao
Institute of Forensic Science
Ministry of Public Security,
Beijing 100038, China

DOI: 10.1002/adfm.201203816

© 2013 WILEY-VCH Verlag GmbH & Co. KGaA, Weinheim

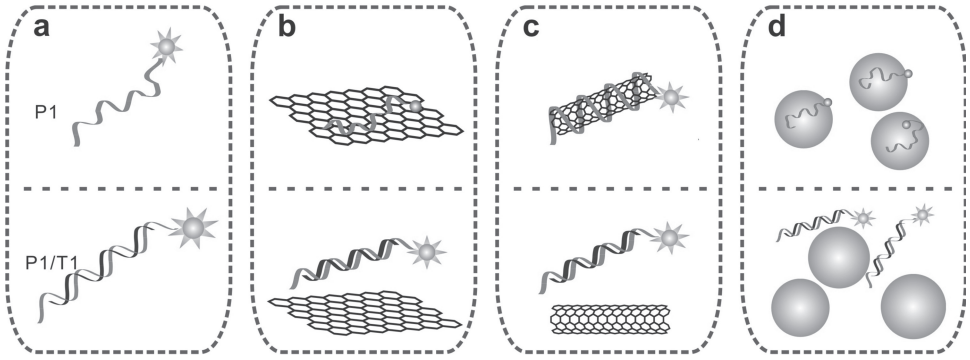

Scheme 1. Scheme for the fluorescent DNA detection based on the DNA hybridization and ssDNA/dsDNA discrimination ability of several nanomaterials. a) The random coiled ssDNA (P1) hybridized with target DNA (T1) and formed strigid dsDNA. b) P1 adsorbed on the surface of GO and the fluorescence of P1 was quenched efficiently, while P1T1 was separate from GO and high fluorescence was maintained. c) The winding of P1 on SWNTs resulted in the high fluorescence quenching while the P1T1 exhibited low affinity to SWNTs. d) P1 adsorbed on the AuNPs surface and resulted in fluorescence quenching of P1; while dsDNA did not.

thermal and mechanical properties,[39,40] which, along with its water-soluble derivative, GO, has become extremely popular in biological applications.[41,42] Previous studies have shown that these three nanomaterials interact differentially with DNA oligonucleotides with different length and structure. A range of fluorescent bioassay methods have been developed based on such properties as well as their superquenching abilities. Particularly, high-sensitivity methods have been developed for sequence-specific detection of DNA hybridization reactions that are of promising applications for diagnostics, antiterrorism, environmental monitoring and forensic analysis.[43–48]

Given the success in constructing these high-sensitivity, high-selectivity assays, it remains unclear whether these three nanomaterials function in the way, which intrigues us to perform a comparative studies on their versatility, limitations, and potential applications. In this study, we have constructed NSET-based bioassays employing AuNPs, SWNTs and GO to detect sequence specific DNA hybridization and investigated operation conditions, kinetics, sensitivity and specificity. We aim to provide guidelines for using these nanomaterials in bioassays, as well as fundamental insights for nanomaterial–biomolecule interactions.

2. Results and Discussion

DNA hybridization provides an ideal model for studying nanomaterial-biomolecule interactions. When DNA oligonucleotides are in the single-stranded (ss-) states, they are very soft polyelectrolytes with random coil-like structures; while the formation of double-stranded (ds-) DNA duplex upon hybridization greatly rigidified the structure. Previous studies with the NSET-based fluorescent assays revealed that there existed different interactions between DNA structures and nanomaterials, with electrostatic and hydrophobic interactions the two primary forces. Here we investigated how fast NMs interact with DNA (adsorption kinetics) and to what extent fluorescence is quenched (thermodynamic quenching efficiency). Two complementary oligonucleotides with the sequences of 5′-FAM-TCG TTG GAG TTT GTC TG-3′ (probe, P1) and 5′-CAG ACA AAC TCC AAC GA-3′ (target, T1) were employed for subsequent studies, with the P1 labeled with a fluorescent dye, FAM. There single-base mismatched sequences of 5′-CAG ACA AA*T* TCC AAC GA-3′ (target, M1), 5′-CAG ACA AA*A* TCC AAC GA-3′ (target, M2) and 5′-CAG ACA AA*G* TCC AAC GA-3′ (target, M3) were used for specificity tests.

2.1. Fluorescence Sensors Bsed on GO, SWNTs and AuNPs

The fluorescence sensors using GO, SWNTs and AuNPs were established by the noncovalent interaction of them and dye-labeled biomolecules[49–53] and the efficient fluorescence quenching of the dye by them.[54–60] The citrate-coated AuNPs have negative charge on the surface,[61] while the chemically dealed SWNTs and GO were also negatively charged and water-dispersible due to the presence of suspended hydroxyl and carboxylic groups at the surface. Otherwise there is a quenching efficiency difference between NMs and FAM-labeled ssDNA and dsDNA. As **Scheme 1** illustrates, ssDNA could bind all three NMs with high affinity while the dsDNA with low affinity, and the dye molecule was pulled close to the surface and quenched efficiently, both of which formed the basis of NMs-based fluorescent sensors. The hybridization of T1 with P1 formed the rigid duplex and resulted in low fluorescence quenching in the presence of NMs due to the weaker interaction between NMs and dsDNA.

We first compared quenching abilities of the three NMs for FAM-labeled P1 and fluorescence restoration after hybridization. Since T1 does not contain a quencher label, hybridization of T1 with P1 formed the rigid duplex while did not lead to substantial variation in fluorescence due to the lack of FRET-based quenching. Interestingly, when the three NMs were added to the solution with oligonucleotides, we found that the fluorescence intensity (FL intensity) was largely modulated, which is consistent with previous reports.

Figure 1 presents the fluorescence change for both ssDNA and dsDNA in presence of three NMs, in which 10 μg/L GO, 20 μg/L SWNTs and 3 nM AuNPs were used. The fluorescence spectra, as well as the quenching efficiency (η) and the signal to noise ratio (S/N), were presented to describe the fluorescence difference induced by those NMs. The fluorescence of P1 was

© 2013 WILEY-VCH Verlag GmbH & Co. KGaA, Weinheim

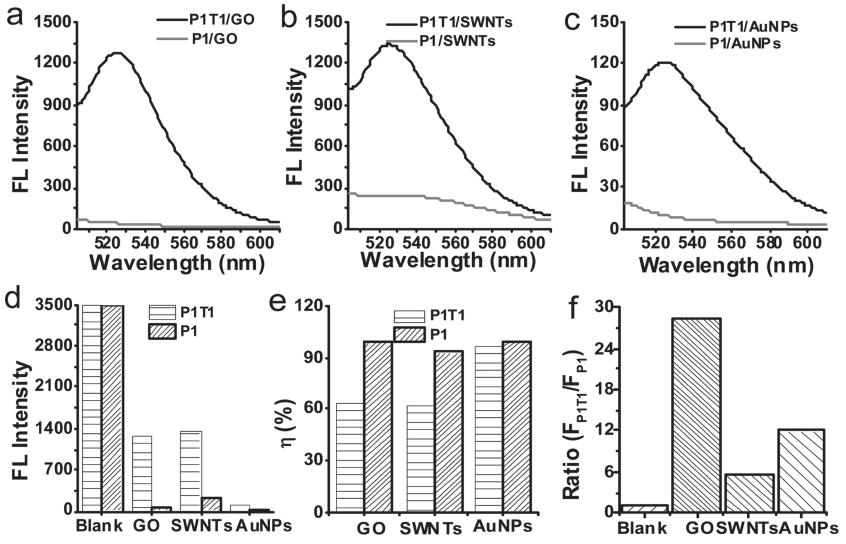

Figure 1. The fluorescence spectra of P1 and P1T1 in the presence of a) GO (10 μg/mL at 20 s), b) SWNTs (20 μg/mL at 60 s), and c) AuNPs (3nM at 10 min). d) The quenching efficiency (η) of three NMs for P1 and P1T1. e) The FL intensity at 525 nm of P1 and P1T1 and f) the FL ratio at 525 nm in the absence and presence of NMs.

nearly totally quenched by GO at 20 s, while that of P1T1 was kept in high level (Figure 1a). Figure 1b illustrates the fluorescence of P1T1 in the presence of SWNTs was similar with that with GO, while the fluorescence of P1 was quenched by SWNTs with relatively low efficiency. different with the quenching behavior of the aforementioned two carbon-based NMs, AuNPs exhibited high quenching ability for both ss- and ds- DNA, and the latter is higher than the former (Figure 1c). In summary, the similar high quenching efficiency for ssDNA in the presence of GO, SWNTs and AuNPs implied their potential use in NSET-based sensor.

Additionally, the FL intensity at 525 nm of P1 and P1T1 in the absence and presence of NMs were listed in Figure 1d, and we could clearly observe the fluorescence change of ss- and ds- DNA induced by three NMs. For all DNA structures in the presence of given concentration of three NMs, the quenching efficiency was calculated by dividing F_{NM}/F_0, where F_0 and F_{NM} are the FL intensity at 525 nm of DNA and DNA-NMs complex, respectively (Figure 1e). As presented in Figure 1d (blank), the fluorescence arising from 20 nM P1 was well maintained after hybridization with 20 nM T1, both of which were set as F_0. The quenching efficiency induce by GO and SWNTs were 63% and 62% for P1T1, which implied the weak GO (SWNTs)-DNA interaction and the consequent low adsorption of P1T1 on the surface of NMs. For P1, 99% and 93% fluorescence were quenched by GO and SWNTs respectively due to the strong GO (SWNTs)-DNA binding. The S/N, presented as F_{P1T1}/F_{P1} in Figure 1d, was calculated, and as high as 28.4 of S/N was obtained in the presence of GO. In contrast, the F_{P1T1}/F_{P1} was 5.6 for SWNTs due to the relatively high background fluorescence from P1 (noise). Interestingly, AuNPs quenched the fluorescence of P1T1 and P1 with high efficiency those were about 97% and 99%, respectively, and the lower fluorescence of P1T1 (signal) led to the lower S/N (12, Figure 1f). Therefore, the highest signal from P1T1 and the lowest noise from P1 led to the highest S/N in the presence of GO, which was considered to be responsible for the best performance of GO-based sensor.

2.2. Fluorescence Quenching Kinetics Analysis

To understand the interaction of different DNA structures with these three NMs, the FL kinetic behaviors of NMs for P1 and P1T1 were studied. **Figure 2**a shows fluorescence quenching of P1 by GO as a function of incubation time. The fluorescence of P1 was quenched very quickly after addition of GO, and the η reached 99% at 20 s. The fluorescence of P1T1 was quenched also quickly in 1 min but with low η (63%). We analyzed the F_{P1T1}/F_{P1} ratio to determine the detection time, and the ratio increased to the highest point (70 times) at 5 min. Since as high as 5 times F_{P1T1}/F_{P1} was achieved after we added GO for 10 s, we could easily detect target DNA at any time point after the addition of GO. Figure 2b illustrated that SWNTs quenched the fluorescence of P1 quickly and more than 96% of fluorescence was quenched after adding SWNTs for 1 min. However, the FL intensity of P1T1 decreased significantly. Therefore, the F_{P1T1}/F_{P1} ratio increased to the highest value (5.3 times) at

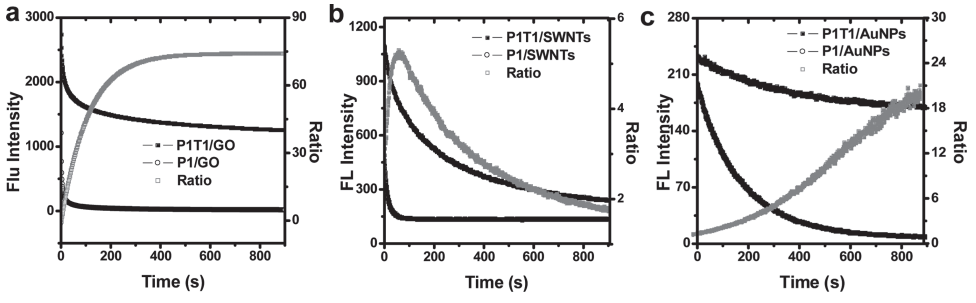

Figure 2. The fluorescence quenching kinetics of NMs for P1 (blue line), P1T1 (black line) and FL ratio at 525 nm in the presence of a) GO, b) SWNTs and c) AuNPs.

© 2013 WILEY-VCH Verlag GmbH & Co. KGaA, Weinheim

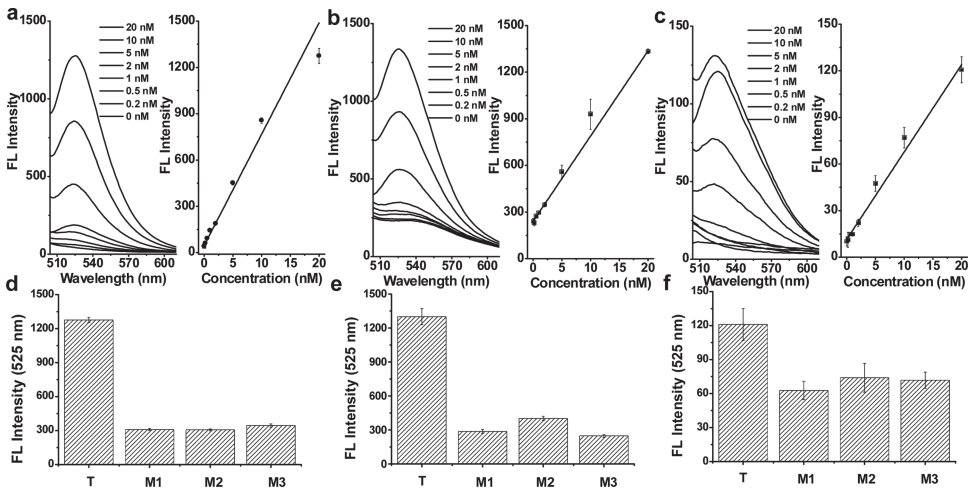

Figure 3. The sensitivity and SNP analysis of three biosensors based on the ssDNA/dsDNA discrimination ability of a,d) GO, b,e) SWNTs and c,f) AuNPs.

1 min, and then a significant decrease appeared with prolonging time due to the steady decrease of F_{P1T1}. In comparison with GO, this SWNTs-based sensor offered a poor target-induced fluorescence restoration and a narrow detection time range, which did not facilitate the sensor's operation. Figure 2c demonstrated that both P1 and P1T1 could be quenched efficiently by 3 nM of AuNPs. The FL intensity of P1 decreased continuously with time prolonging and reached background level, and the F_{P1T1}/F_{P1} ratio reached to 20 times at 15 min. Comprehensively considering the kinetics and quenching efficiency of these three NMs, the GO-based sensor offered the best performance with highest target-induced fluorescence restoration (70 times) and fastest kinetics (within 1 min).

2.3. Performance of NM-Based Sensors

Based on the quenching efficiency and kinetics analysis, we believe the GO-based sensor possess best performance among three NMs. **Figure 3** listed the sensitivity and selectivity of these three different NMs-based sensors, in which 20 nM of P1 and optimized concentrations for each NM (10 μg/mL of GO, 20 μg/mL of SWNTS, and 3 nM of AuNPs; see Supporting Information) were used to detect 0-40 nM of T1. The fluorescence signal exhibited good linear relation with increasing T1 concentration for three sensors, however GO-based sensor exhibited best sensitivity (limit of detection, LOD: 0.2 nM) and repeatability (relative standard deviation RSD: 0.5%–4%) in the linear range from 0 to 20 nM (Figure 3a). SWNTs- and AuNPs-based sensors possess similar sensitivity that is in a nanomolar level (Figure 3b,c) with higher LOD of 1 nM (SWNTs group) and 2 nM (AuNPs group). The SNPs analysis were performed and demonstrated in Figure 3d–f. GO- and SWNT-based sensors exhibited excellent discrimination of single mismatch base pairs from perfect matched sequences, and the fluorescence ratio (F_{P1T1}/F_{P1M1}) (**Table 1**) was as high as 4. The AuNPs exhibited poor discrimination ability and the ratio located in the range of 1–2.

Table 1. Performance comparison of three NMs-based sensors.

		GO	SWNTs	AuNPs
LOD		0.2 nM	1 nM	2 nM
SNP	F_{P1T1}/F_{P1M1}	4.1	4.5	1.9
	F_{P1T1}/F_{P1M2}	4.2	3.2	1.6
	F_{P1T1}/F_{P1M3}	3.7	5.3	1.7
RSD = SD/Mean (%)		0.5–3.8	1.5–10.4	2.3–43.4
Optimized detection time		20 s	1 min	15 min

2.4. Mechanisms of Nanomaterial–DNA Interactions

We have shown that GO exhibited the highest quenching efficiency, fastest binding kinetics with DNA molecules, and best discrimination ability for different structures of DNA (including ssDNA, dsDNA, and mismatched sequence). Consequently, the GO-based sensor possessed highest sensitivity and specificity and best repeatability those were required by a reliable assay in most detection event especially for clinical medical application. As is known, AuNPs are 0D metallic nanoparticles with 13 nm diameter, while SWNTs and GO are 1D and 2D carbon nanomaterials with one-atom thick (about 1 nm), and the surface of all these three NMs are negatively charged. Considering of their component and surface charge, as well as size and shape, we believe the performance of these three sensors is highly correlated with their physical and chemical properties and unique nanometer size.

We first analyzed the occupied space (footprint) and the distribution of ssDNA on the surface of three NMs. The optimized quantity of three NMs in the assay was investigated for gaining the respective highest performance, and we then detailed analyzed the influence of NMs' quantity to the quenching behavior and kinetics were presented in **Figure 4** and Supporting Information (Figure S2–S4). The surface area of NMs with optimized quantity (3 nM for AuNPs, 20 μg/mL for SWNTs, and 5 μg/mL for GO), as well as the ssDNA density on the surface

© 2013 WILEY-VCH Verlag GmbH & Co. KGaA, Weinheim

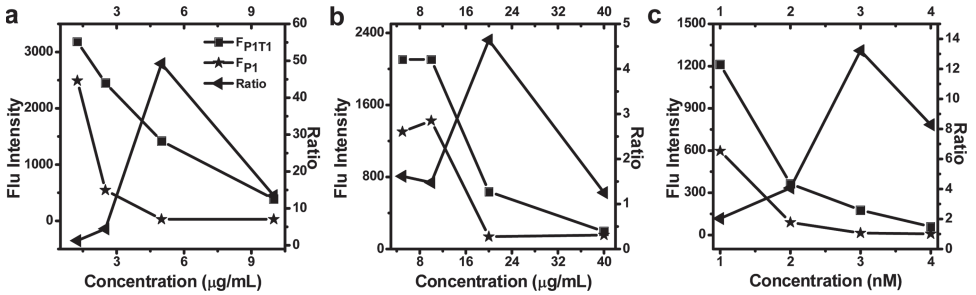

Figure 4. Effects of different concentration of a) GO, b) SWNTs, and c) AuNPs on fluorescence quenching. Left: FL intensity at 525 nm; Right: F_{P1T1}/F_{P1}. a) GO concentrations: 1.25, 2.5, 5, 10 μg/mL. b) SWNTs concentrations: 5, 10, 20, 40 μg/mL. c) AuNP concentrations: 1.1, 2.3, 3.5, 4.6 nM.

and the surface coverage of ssDNA were calculated and listed in **Table 2**. GO possesses similar surface area (112 cm^2) with SWNTs (154 cm^2), which is larger than AuNPs (38.4 cm^2). After addition of 20 nM P1, the ssDNA density on the surface of GO, SWNTs, and AuNPs were $1.1 \times 10^{11}/cm^2$, $7.8 \times 10^{10}/cm^2$, and $3.1 \times 10^{11}/cm^2$, respectively. Among them, AuNPs possess the highest ssDNA density, which was considered to be related with its 0D shape and the large outer space for DNA stretching. Worthy of noting, the surface coverage of ssDNA for all NMs is very low, which implies all DNA molecules have enough room to bind the surface and thus leads to the similar high quenching efficiency of three NMs. For example, the fluorescence of ssDNA was efficiently quenched when the concentration of GO reached 5 μg/mL, and the surface coverage is 0.19%. However, when the surface coverage increased to 0.38% by employing 2.5 μg/mL GO, some unbound ssDNA remained in solution and led to high fluorescence background. The ultralow surface coverage of ssDNA was considered to be associated with the negatively charged surface of NMs and DNA. It is known that ssDNA is an amphoteric molecule with positively charged bases and a negatively charged phosphate bone. The binding of ssDNA on the surface increased the negative charge density of AuNPs, and the electrostatic repulsion between ssDNA-covered NMs and ssDNA blocked further binding of free ssDNA molecules in solution on the NMs' surface, and thus resulted in the low surface coverage of ssDNA. This phenomenon was similar for SWNTs and AuNPs, thus the quenching efficiencies were kept in high level because all DNA molecules have sufficient room to anchor. Despite of the similar quenching efficiency, these sensors exhibited different kinetics, repeatability, and single-mismatch differentiation. We believe those characters are greatly associated with the interaction between NMs and DNA molecules.

Table 2. Various properties of NMs.

		AuNPs	SWNTs[a)]	GO[a)]
Total surface area[a)]		38.4 cm^2	154 cm^2	112 cm^2
ssDNA surface density[a)]		$3.1 \times 10^{11}/cm^2$	$7.8 \times 10^{10}/cm^2$	$1.1 \times 10^{11}/cm^2$
Surface coverage[a)]		0.55%	0.14%	0.19%
Z-potential (mV)	in water	–35.7	–31	–43
	in PBS[b)]	–32.7	–23.5	–24.6
Interaction mode		Electrostatic Au-N	Electrostatic π-π stacking and cation-π	Electrostatic π-π stacking and cation-π

[a)]See Supporting Information; [b)]0.1 mg/mL GO and SWNTs were determined in 0.1 M PBS, while 2 nM AuNPs in 30 mM PBS.

In our study, we found that salt concentration greatly influenced the NMs-DNA interaction and consequent quenching efficiency and kinetics and SNP differentiation etc. The FL intensity at 525 nm of ssDNA and dsDNA at various concentrations of NaCl, as well as their ratio, as a function of time were demonstrated in Supporting Information Figure S5–S7. The quenching efficiency of NMs for both ssDNA and dsDNA increased along with the rising NaCl concentration, and the optimized NaCl concentration was achieved as 100 mM for GO and SWNTs whereas 30 mM for AuNPs when the FL ratio was highest. Since NaCl concentration is generally employed to screen the charge-induced intermolecular repulsion in DNA hybridization and other electrostatic-dominated processes, here we believe the electrostatic force play a dominate role in the NMs-DNA interaction, and the adsorption kinetics and binding capacity could be improved by modulating NaCl concentration. For all three negatively charged NMs, their Z-potentials (ZP) in aqueous solution were determined to estimate the surface charge status of NMs and analyze the electrostatic interaction between DNA and NMs. As listed in Table 2, the ZPs of AuNPs, SWNTs and GO in Milli Q water were –35.7, –31, and –43 mV, respectively; illustrating these NMs have good stability in aqueous solution and high affinity with positive charged molecules and groups. Considering the close relationship of ZP with electrolyte concentration, the ZPs of three NMs in their each optimized buffer were also determined. And 2 nM AuNPs in 30 mM PBS shows the highest ZP as –32.7 mV; whereas 0.1 mg/mL GO and SWNTs in 100 mM PBS exhibits similar values lower than AuNPs (–24.6 mV for GO and –23.5 mV for SWNTs). This phenomenon was in good agreement with the charge screening effect arising from salt, and the lower salt concentration (30 mM) resulted minimal change of ZP (3 mV) compared with SWNTs (7.5 mV) and GO (18.4 mV) in 100 mM PB. As is known, the negatively charged surface of NMs favored the attractive binding of positively charged nucleobases hanging out of ssDNA with NMs and disfavored that of phosphate backbones of ssDNA and dsDNA.[62–64] Therefore, the adsorption behavior of dsDNA possessing higher charge density on the surface of NMs was more than ready to be regulated

© 2013 WILEY-VCH Verlag GmbH & Co. KGaA, Weinheim

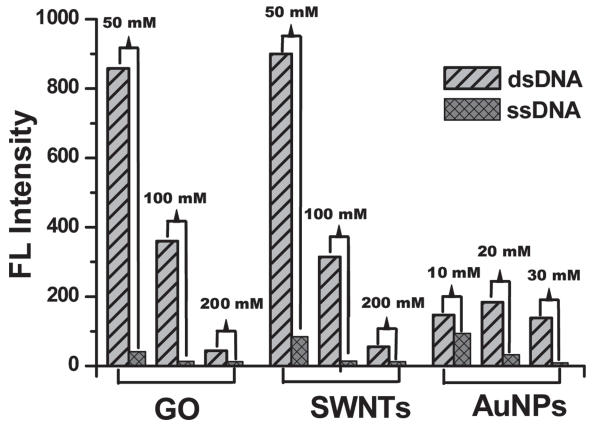

Figure 5. FL intensity of DNA in the presence of different concentrations of NaCl. The fluorescence was collected at 525 nm and 300 s and the background fluorescence was subtracted.

by salt concentration, and higher salt concentration led to more effect on NMs-dsDNA. **Figure 5** presented the fluorescence of DNA at 525 nm with different NaCl concentrations in the presence of NMs, and the dramatic decline of the fluorescence of dsDNA in the presence of GO appeared as NaCl increased from 50 to 200 mM, which is not same as ssDNA.

Despite of the electrostatic repulsion, other attractive force were involved in the NMs-DNA interaction to achieve stable adsorption of DNA on NMs. The Au-N donor-acceptor bond, with 0.2 eV bond energy,[65] worked for Au-nucleobase binding, and each base bound to Au surface with 3–4 N-containing contact points.[66] While for GO and SWNTs with single graphene layer, previous studies approved that nucleobases and aromatic compounds could bind them through π–π stacking mode,[33,67–71] and as high as 0.6–0.8 eV bond energy and multi-contact points of long stands favored the tight binding of ssDNA with GO.[72] This was consistent with the results in Supporting Information Figure S5, in which the fluorescence of ssDNA was efficiently quenched when NaCl was 50, 100, and 200 mM. However, there was also a sharp decline for the fluorescence of dsDNA along with the increasing NaCl, implying dsDNA could also strongly adsorb on NMs. This was contrary to our previous reports, in which dsDNA was considered to be apart from GO and their fluorescence was well maintained. This salt-dependent adsorption might be explained by the cation-π interaction between GO and dsDNA. Cation-π interaction is a noncovalent molecular interaction between the face of an electron-rich π system with an adjacent cation.[73,74] GO is known as a big π^- system, while DNA is a polyelectrolyte with negative-charged phosphate backbone and π-conjugated nucleobases, both of which possess prerequisite for forming cation-π. First, the counterions (Na^+) adsorbed on the GO's surface through cation-π interaction with an adsorption energy of 1.0–1.2 eV,[75] and then sodium ions in the large π system attracted negative-charged dsDNA and formed stable dsDNA-GO complexes. Reasonably, cation-π interaction could be regulated by salt concentration and the higher concentration of counterions led to stronger cation-π interaction. As mentioned earlier, both electrostatic and induction energies dominated the metal cation-mediated cation-π interaction,[76–78] thus the salt-dependent character of electrostatic interaction is also suitable for explaining cation-π interaction. Of the three NMs, the carbon-based GO and SWNTs exhibited faster kinetics and higher performance, which was considered to be determined by the higher bond energy from cation-π and π–π stacking.

Another considerable factor was the shape and the size, which offered different curvatures.[79] The 0D AuNPs have the highest curvature, and then 1D SWNTs, and lastly 2D GO. As we know, the higher curvature, the higher energy was consumed for the adsorbed molecules to bind. For 0D AuNPs, the adsorbed molecules should bent significantly to bind on the spherical surface. In another respect, a few nucleobases of ssDNA bind on the surface of particle immediately, and then desorption and re-adsorption process occurred to reach the thermodynamic balance of adsorption. These factors make the adsorption slower than GO and SWNTs. For SWNTs, the similar thermodynamic balance process would occur on the curving sidewall of SWNT, which contribute to the lower ssDNA adsorption in comparison with GO.

It is worth noting that the stronger interaction (including hydrogen bond and π-stacking) of bases in duplex DNA[80] than in DNA-NMs complex leads to the competitive displacement of P1 from NMs' surface and hybridization with T1, which formed the basis of DNA sensor based on the NMs-DNA interaction. By analyzing the interaction mode and intensity, the GO-based sensor exhibited the highest binding kinetics and repeatability due to the size and the characteristic GO-DNA interaction. Furthermore, the strong interaction of ssDNA and GO facilitated the unwinding of loose duplex composed of mismatched sequence thus resulted in excellent SNP discrimination (Figure 3d).

3. Conclusions

In this work, three types of nanomaterials, 0D AuNPs, 1D SWNTs, and 2D GO, and their characterized interaction with DNA were investigated detailed for well understanding their characters and designing sensing strategies. The fluorescence quenching behavior of NMs, the performance of three NMs-based sensors, and the NMs-DNA interaction were well studied here. The fluorescence quenching experiments approved that all three NMs possess high quenching efficiency for Fam-labeled ssDNA, and 99%, 96% and 99% of fluorescence were quenched by GO, SWNTs and AuNPs. Whereas, the fluorescence ratio of ds- and ss- DNA were presented as 28.4, 5.6, and 12, implying the highest differentiation of ssDNA and dsDNA were achieved by employing GO. Consequently, the GO-based sensor exhibited the best sensitivity (LOD: 0.2 nM) and repeatability in the linear range from 0 to 20 nM target DNA, while 1 nM of LOD for SWNTs group and 2 nM for AuNPs group. Worthy of noting, GO- and SWNTs-based sensors exhibited excellent discrimination of single mismatch base pairs from perfect matched sequences, and over four times fluorescence decrease arising from single mismatch employing GO and SWNTs. More importantly, the related mechanisms were carefully analyzed through investigating the use of NMs and the concentration of NaCl. The surface coverage of ssDNA, the

© 2013 WILEY-VCH Verlag GmbH & Co. KGaA, Weinheim

Table 3. Sequences of oligonucleotides.

Name	Sequences
P1 (Probe sequence)	5′-FAM-TCG TTG GAG TTT GTC TG-3′
T1 (Target sequence)	5′-CAG ACA AAC TCC AAC GA-3′
R1 (Random sequence)	5′-GCA GAG CCA GTT CCA AG-3′
M1 (mismatch sequence-1)	5′-CAG ACA AA*T* TCC AAC GA-3′
M2 (mismatch sequence-2)	5′-CAG ACA AA*A* TCC AAC GA-3′
M3 (mismatch sequence-3)	5′-CAG ACA AA*G* TCC AAC GA-3′

characterized interaction between NMs and DNA, as well as the curvature of NMs were highly associated with the performance of NMs-based sensor. AuNPs exhibited highest surface coverage of ssDNA, highest Z potential in operating solution (implying the highest electrostatic force) and lowest Au-N bond, and all of them are responsible for the highest dsDNA quenching and consequent low performance of DNA detection. For both carbon-based NMs, similar interaction and surface coverage, as well as the different curvature results in the better performance of GO-based sensor. We believe this work will offer guidance for the choice of NMs and elaborate design of biosensors.

4. Experimental Section

Materials: SWNTs were purchased from Sigma Corporation. Graphite powder and hydrogen tetrachloroaurate (III) ($HAuCl_4{\cdot}4H_2O$, 99.99%) were purchased from China National Pharmaceutical Group Corporation. All other chemicals were of analytical grade. All chemicals were used without further purification. Milli Q Water was used for the whole procedure. DNA oligonucleotides were synthesized and purified by HPLC (Sangon Biotechnology Inc., Shanghai). The sequences of the involved oligonucleotides are listed in **Table 3**.

AuNP Preparation: AuNPs of 15 nm were synthesized by citrate reduction of $HAuCl_4$ as reported elsewhere; briefly, 4 mL of 1% trisodium citrate solution was added to a boiling, rapidly stirred solution of 1% $HAuCl_4$. The solution was kept boiling and stirred for 20 min. After being cooled to room temperature, the prepared AuNPs were stored at 4 °C. Prepared AuNPs were concentrated from about 2.3 nM to about 11.5 nM AuNPs for further use in this work. Different concentrations of AuNPs were obtained by diluting 11.5 nM AuNPs solution with various volume of AuNPs buffer.

Preparation of GO: Based on the Hummer's method, GO was synthesized from graphite powder.[81] Briefly, a conical flask equipped with a magnetic stirring bar was charged with 20 mL concentrated H_2SO_4 containing $K_2S_2O_8$ (8 g), and P_2O_5 (8 g). Then graphite power (4 g) was added into the solution at 80 °C. After stirred over 6 h, the resulting dark blue mixture was thermally isolated and slowly cooled to room temperature. The mixture was poured into 300 mL of water, and the solution was filtrated with a filter membrane of 0.22 μm (Generay Biotech Co., Ltd., Shanghai, China) and dried overnight at 60 °C. These preoxidized graphite powder (2 g) was added to 92 mL of cold H_2SO_4 (0 °C), to which $KMnO_4$ (12 g) was gradually added under continuous stirring in ice-bath. After 15 min, $NaNO_3$ (2 g) was added to the mixture. The solution was further stirred for 2 h at 35 °C and distilled water (200 mL) was added. The mixture was poured into 560 mL of water, after which 10 mL of H_2O_2 (30%) was slowly added. The product was washed with HCl (1:10) and then filtered. The material was redispersed in water and washed with water until the pH of the filtrate was neutral. The brown dispersion was extensively dialyzed to remove residual metal ions and acids, and then exfoliated via sonication for 1.5 h (300 W). Unexfoliated graphite oxide was removed by centrifugation (3000 rpm, 5 min) using Centrifuge himac-CF 16RX (Hitachi, Japan). The as-prepared GO sample (0.5 mg/mL) was then characterized with tapping-mode atomic force microscope (AFM).[42,82]

Preparation of SWNTs: The SWNTs for this study were prepared based on Richard E. Smalley's method.[83] SWNTs (100 mg) were dipped into 50 mL of concentrated HCl overnight. The product was wash with distilled water as far as water was neutral, and then filtrated with a filter membrane of 0.22 μm (Generay Biotech Co., Ltd., Shanghai, China) and dried overnight at 60 °C. The dry SWNTs were added into 50 mL of 3:1 concentrated H_2SO_4:HNO_3 mixture under continuous stirring with 80 °C for 8 h. In the same way, the product was wash with Milli Q Water as far as water was neutral, and dried. At last the SWNTs were suspended in distilled water with concentration of 1 mg/mL for further use in this work.

Fluorescence Assays: Fluorescence spectra were measured on a fluorometer (Hitachi F-4500 Fluorescence spectrophotometer). In optimizing concentrations of NMs, the fluorescent probe 1 (P1, 20 nM) were hybridized with the target sequence (T1, 20 nM) or random sequence (R1, 20 nM) in 500 μL hybridization buffer (100 mM NaCl, 10 mM PB, pH 7.4) for 10 min under 37 °C. In fluorescence quenching assay, 1 mL mixture of the hybridization buffer (100 mM NaCl, 10 mM PB, pH 7.4) with different volumes of GO solution (0.5 mg/mL) of 2.5 μL, 5 μL, 10 μL, 20 μL or SWNTs solution (1 mg/mL) of 5 μL, 10 μL, 20 μL,40 μL were added, and the added solution in AuNPs assay were the 500 μL mixture of H_2O with different volumes of AuNPs solution (10 nM) of 100 μL, 200 μL, 300 μL, 400 μL.

In optimizing concentrations of NaCl of detection buffer assay, the fluorescent probe 1 (P1, 20 nM) were hybridized with the target sequence (T1, 20 nM) or random sequence (R1, 20 nM) in 100 μL hybridizer buffer (100 mM NaCl, 10 mM PB, pH 7.4) for 10 min under 37 °C. In fluorescence quenching assay, the concentration of NaCl in final detection buffer were adjusted to 50 mM, 100 mM, 200 mM for GO- and SWNTs-based assays, and 10 μg/mL of GO or 20 μg/mL of SWNTs was used; while 20 mM, 30 mM, 40 mM of NaCl was used for AuNPs-based assay by adding different volumes of the buffer of 1 M NaCl, 10 mM PB, pH 7.4, and 3 nM of AuNPs was used.

In the concentration gradient assay, the fluorescent P1 (20 nM) were hybridized with the different concentration T1 of 0 nM, 0.2 nM, 0.5 nM, 1 nM, 2 nM, 5 nM, 10 nM, 20 nM and 40 nM for 10 min under 37 °C. 10 μg/mL of GO and 100 mM NaCl were used for T1 detection. The fluorescence spectra were recorded at 45 s after GO added with excitation and emission wavelength of 494 nm and 524 nm, respectively. 20 μg/mL of SWNTs and 100 mM of NaCl were used for T1 detection. The fluorescence spectra were recorded at 100 s after SWNTs added. And 3 nM AuNPs and 40 mM NaCl were used and the fluorescence spectra were recorded at 15 min after AuNPs added. For the SNP assay, the fluorescent P1 (20 nM) were hybridized with the different mismatch sequences of M1, M2 and M3 with 20 nM for 10 min under 45 °C, and all the procedures are in accordance with sensitivity analysis.

Supporting Information

Supporting Information is available from the Wiley Online Library or from the author.

Acknowledgements

This work was supported by the National Basic Research Program of China (973 program, 2013CB933800, 2012CB825805, 2012CB932600), NSFC (21077321, 21105028, 21227804), CAS (KJCX2-EWN03) and K. C. Wong education foundation, Hong Kong.

Received: December 22, 2012
Published online: March 22, 2013

© 2013 WILEY-VCH Verlag GmbH & Co. KGaA, Weinheim

[1] P. M. Holland, R. D. Abramson, R. Watson, D. H. Gelfand, *Proc. Natl. Acad. Sci. USA* **1991**, *88*, 7276.
[2] S. Tyagi, F. Kramer, *Nat. Biotechnol.* **1996**, *14*, 303.
[3] C. J. Yang, C. D. Medley, W. H. Tan, *Curr. Pharm. Biotechnol.* **2005**, *6*, 445.
[4] S. D. Jhaveri, R. Kirby, R. Conrad, E. J. Maglott, M. Bowser, R. T. Kennedy, G. Glick, A. D. Ellington, *J. Am. Chem. Soc.* **2000**, *122*, 2469.
[5] R. Nutiu, Y. Li, *Methods* **2005**, *37*, 16.
[6] P. Alivisatos, *Nat. Biotechnol.* **2004**, *22*, 47.
[7] E. Katz, I. Willner, *Angew. Chem. Int. Ed.* **2004**, *43*, 6042.
[8] J. Xiang, W. Lu, Y. Hu, Y. Wu, H. Yan, C. M. Lieber, *Nature* **2006**, *441*, 489.
[9] J.-M. Nam, C. S. Thaxton, C. A. Mirkin, *Science* **2003**, *301*, 1884.
[10] X. Gao, Y. Cui, R. M. Levenson, L. W. K. Chung, S. Nie, *Nat. Biotechnol.* **2004**, *22*, 969.
[11] P. C. Ray, *Angew. Chem. Int. Ed.* **2006**, *45*, 1151.
[12] L. Q. Chu, R. Förch, W. Knoll, *Angew. Chem. Int. Ed.* **2007**, *46*, 4944.
[13] T. N. Grossmann, L. Röglin, O. Seitz, *Angew. Chem. Int. Ed.* **2007**, *46*, 5223.
[14] X. Huang, I. H. El-Sayed, W. Qian, M. A. El-Sayed, *Nano Lett.* **2007**, *7*, 1591.
[15] G. H. Chan, J. Zhao, E. M. Hicks, G. C. Schatz, R. P. Van Duyne, *Nano Lett.* **2007**, *7*, 1947.
[16] X. Huang, I. H. El-Sayed, W. Qian, M. A. El-Sayed, *J. Am. Chem. Soc.* **2006**, *128*, 2115.
[17] B. P. Khanal, E. R. Zubarev, *Angew. Chem. Int. Ed.* **2007**, *46*, 2195.
[18] H. Liao, C. L. Nehl, J. H. Hafner, *Nanomedicine* **2006**, *1*, 201.
[19] V. Berry, S. Rangaswamy, R. F. Saraf, *Nano Lett.* **2004**, *4*, 939.
[20] V. Berry, A. Gole, S. Kundu, C. J. Murphy, R. F. Saraf, *J. Am. Chem. Soc.* **2005**, *127*, 17600.
[21] F. Patolsky, G. Zheng, C. M. Lieber, *Anal. Chem.* **2006**, *78*, 4260.
[22] Y. Cui, Q. Wei, H. Park, C. M. Lieber, *Science* **2001**, *293*, 1289.
[23] H. Cai, X. Cao, Y. Jiang, P. He, Y. Fang, *Anal. Bioanal. Chem.* **2003**, *375*, 287.
[24] H. Cai, C. Xu, P. He, Y. Fang, *J. Electroanal. Chem.* **2001**, *510*, 78.
[25] J. D. Le, Y. Pinto, N. C. Seeman, K. Musier-Forsyth, T. A. Taton, R. A. Kiehl, *Nano Lett.* **2004**, *4*, 2343.
[26] C.-C. Huang, Z. Yang, K.-H. Lee, H.-T. Chang, *Angew. Chem. Int. Ed.* **2007**, *46*, 6824.
[27] P. C. Ray, A. Fortner, G. K. Darbha, *J. Phys. Chem. B* **2006**, *110*, 20745.
[28] T. L. Jennings, M. P. Singh, G. F. Strouse, *J. Am. Chem. Soc.* **2006**, *128*, 5462.
[29] P. C. Ray, G. K Darbha, A. Ray, W. Hardy. J. Walker, *Nanotechnology* **2007**, *18*, 375504.
[30] B. Dubertret, M. Calame, A. J. Libchaber, *Nat. Biotechnol.* **2001**, *19*, 365.
[31] D. J. Maxwell, J. R. Taylor, S. Nie, *J. Am. Chem. Soc.* **2002**, *124*, 9606.
[32] D. S. Seferos, D. A. Giljohann, H. D. Hill, A. E. Prigodich, C. A. Mirkin, *J. Am. Chem. Soc.* **2007**, *129*, 15477.
[33] R. Yang, J. Jin, Y. Chen, N. Shao, H. Kang, Z. Xiao, Z. Tang, Y. Wu, Z. Zhu, W. Tan, *J. Am. Chem. Soc.* **2008**, *130*, 8351.
[34] R. Elghanian, J. J. Storhoff, R. C. Mucic, R. L. Letsinger, C. A. Mirkin, *Science* **1997**, *277*, 1078.
[35] J. Li, S. Song, X. Liu, L. Wang, D. Pan, Q. Huang, Y. Zhao, C. Fan, *Adv. Mater.* **2008**, *20*, 497.
[36] Z. Liu, X. Sun, N. Nakayama-Ratchford, H. Dai, *ACS Nano* **2007**, *1*, 50.
[37] K. Besteman, J.-O. Lee, F. G. M. Wiertz, H. A. Heering, C. Dekker, *Nano Lett.* **2003**, *3*, 727.
[38] X. Tang, S. Bansaruntip, N. Nakayama, E. Yenilmez, Y.-l. Chang, Q. Wang, *Nano Lett.* **2006**, *6*, 1632.
[39] D. Li, R. B. Kaner, *Science* **2008**, *320*, 1170.
[40] K. S. Novoselov, A. K. Geim, S. V. Morozov, D. Jiang, Y. Zhang, S. V. Dubonos, I. V. Grigorieva, A. A. Firsov, *Science* **2004**, *306*, 666.
[41] N. Mohanty, V. Berry, *Nano Lett.* **2008**, *8*, 4469.
[42] X. Sun, Z. Liu, K. Welsher, J. Robinson, A. Goodwin, S. Zaric, H. Dai, *Nano Res.* **2008**, *1*, 203.
[43] G. Hanrahan, D. G. Patil, J. Wang, *J. Environ. Monit.* **2004**, *6*, 657.
[44] C. Debouck, P. N. Goodfellow, *Nat. Genet.* **1999**, *21*, 48.
[45] T. A. Taton, C. A. Mirkin, R. L. Letsinger, *Science* **2000**, *289*, 1757.
[46] C. Fan, K. W. Plaxco, A. J. Heeger, *Proc. Natl. Acad. Sci. USA* **2003**, *100*, 9134.
[47] F. Patolsky, A. Lichtenstein, I. Willner, *J. Am. Chem. Soc.* **1999**, *122*, 418.
[48] F. Höök, A. Ray, B. Nordén, B. Kasemo, *Langmuir* **2001**, *17*, 8305.
[49] P. J. Boul, D.-G. Cho, G. M. Rahman, A. M. Marquez, Z. Ou, K. M. Kadish, D. M. Guldi, J. L. Sessler, *J. Am. Chem. Soc.* **2007**, *129*, 5683.
[50] N. Nakayama-Ratchford, S. Bangsaruntip, X. Sun, K. Welsher, H. J. Dai, *J. Am. Chem. Soc.* **2007**, *129*, 2448.
[51] H. Li, B. Zhou, Y. Lin, L. Gu, W. Wang, K. A. S. Fernando, S. Kumar, L. F. Allard, Y.-P. Sun, *J. Am. Chem. Soc.* **2004**, *126*, 1014.
[52] E. S. Jeng, A. E. Moll, A. C. Roy, J. B. Gastala, M. S. Strano, *Nano Lett.* **2006**, *6*, 371.
[53] N. W. S. Kim, O'Connell, M. J. A. Wisdom, H. J. Dai, *Proc. Natl. Acad. Sci. USA* **2005**, *102*, 11600.
[54] C. Fan, S. Wang, J. W. Hong, G. C. Bazan, K. W. Plaxco, A. J. Heeger, *Proc. Natl. Acad. Sci. USA* **2003**, *100*, 6297.
[55] E. Dulkeith, A. C. Morteani, T. Niedereichholz, T. A. Klar, J. Feldmann, S. A. Levi, F. C. van Veggel, D. N. Reinhoudt, M. MÖller, D. I. Gittins, *Phys. Rev. Lett.* **2002**, *89*, 203002.
[56] D. A. Britz, A. N. Khlobystov, *Chem. Soc. Rev.* **2006**, *35*, 637.
[57] E. Dulkeith, M. Ringler, T. A. Klar, J. Feldmann, A. Muñoz Javier, W. J. Parak, *Nano Lett.* **2005**, *5*, 585.
[58] E. Treossi, M. Melucci, A. Liscio, M. Gazzano, P. Samori, V. Palermo, *J. Am. Chem. Soc.* **2009**, *131*, 15576.
[59] E. S. Cho, S. W. Hong, W. H. Jo, *Macro. Rapid Commun.* **2008**, *29*, 1798.
[60] J. Kim, L. J. Cote, F. Kim, J. Huang, *J. Am. Chem. Soc.* **2009**, *132*, 260.
[61] Huixiang Li, Lewis J. Rothberg, *Anal. Chem.* **2004**, *76*, 5414.
[62] D. Li, S. Song, C. Fan, *Acc. Chem. Res.* **2010**, *43*, 631.
[63] L. Wang, X. Liu, X. Hu, S. Song, C. Fan, *Chem. Commun.* **2006**, 3780.
[64] X. Zhang, M. R. Servos, J. Liu, *Langmuir* **2012**, *28*, 3896.
[65] M. Frei, S. V. Aradhya, M. Koentopp, M. S. Hybertsen, L. Venkataraman, *Nano Lett.* **2011**, *11*, 1518.
[66] J. Liu, *Phys. Chem. Chem. Phys.* **2012**, *14*, 10485.
[67] M. Zheng, A. Jagota, M. S. Strano, A. P. Santos, P. Barone, S. G. Chou, B. A. Diner, M. S. Dresselhaus, R. S. McLean, G. B. Onoa, G. G. Samsonidze, E. D. Semke, M. Usrey, D. J. Walls, *Science* **2003**, *302*, 1545.
[68] S. Wang, E. S. Humphreys, S.-Y. Chung, D. F. Delduco, S. R. Lustig, H. Wang, K. N. Parker, N. W. Rizzo, S. Subramoney, Y.-M. Chiang, A. Jagota, *Nat. Mater.* **2003**, *2*, 196.
[69] Z. Liu, J. T. Robinson, X. Sun, H. Dai, *J. Am. Chem. Soc.* **2008**, *130*, 10876.
[70] N. Mohanty, U. Mogera, A. Govindaraj, A. Das, P. K. Maiti, A. K. Sood, C. N. R. Rao, *ChemPhysChem* **2009**, *10*, 206.
[71] M. Zheng, A. Jagota, E. D. Semke, B. A. Diner, R. S. McLean, S. R. Lustig, R. E. Richardson, N. G. Tassi, *Nat. Mater.* **2003**, *2*, 338.
[72] B. Song, G. Cuniberti, S. Sanvito, H. Fang, *Appl. Phys. Lett.* **2012**, *100*, 063101.
[73] D. Umadevi, G. N. Sastry, *J. Phys. Chem. C* **2011**, *115*, 9656.
[74] D. Umadevi, G. N. Sastry, *J. Phys. Chem. C* **2011**, *115*, 9656.

© 2013 WILEY-VCH Verlag GmbH & Co. KGaA, Weinheim

[75] F. Valencia, A. H. Romero, F. Ancilotto, P. L. Silvestrelli, *J. Phys. Chem. B* **2006**, *110*, 14832.
[76] V. Georgakilas, M. Otyepka, A. B. Bourlinos, V. Chandra, N. Kim, K. C. Kemp, P. Hobza, R. Zboril, K. S. Kim, *Chem. Rev.* **2012**, *112*, 6156.
[77] D. A. Dougherty, D. A. Stauffer, *Science* **1990**, *250*, 1558.
[78] D. Kim, S. Hu, P. Tarakeshwar, K. S. Kim, J. M. Lisy, *J. Phys. Chem. A* **2003**, *107*, 1228.
[79] M.-C. Daniel, I. B. Tsvetkova, Z. T. Quinkert, A. Murali, M. De, V. M. Rotello, C. C. Kao, B. Dragnea, *ACS Nano* **2010**, *4*, 3853.
[80] C. F. Matta, N. Castillo, R. J. Boyd, *J. Phys. Chem. B* **2005**, *110*, 563.
[81] W. S. Hummers, R. E. Offeman, *J. Am. Chem. Soc.* **1958**, *80*, 1339.
[82] D. Li, M. B. Müller, S. Gilje, R. B. Kaner, G. G. Wallace, *Nat. Nanotechnol.* **2008**, *3*, 101.
[83] J. Liu, A. G. Rinzler, H. Dai, J. H. Hafner, R. K. Bradley, P. J. Boul, A. Lu, T. Iverson, K. Shelimov, C. B. Huffman, F. Rodriguez-Macias, Y.-S. Shon, T. R. Lee, D. T. Colbert, R. E. Smalley, *Science* **1998**, *280*, 1253.

© 2013 WILEY-VCH Verlag GmbH & Co. KGaA, Weinheim